PCCP

Accepted Manuscript

ROYAL SOCIETY OF CHEMISTRY

www.rsc.org/pccp

Non-Fullerene Acceptors: Exciton Dissociation with PTCDA versus C_{60}

Gregory. J. Dutton and Steven. W. Robey*

National Institute of Standards and Technology,
100 Bureau Dr., Gaithersburg, MD 20899

Abstract

Extensive development of new polymer and small molecule donors has helped produce a steady increase in the efficiency of organic photovoltaic (OPV) devices. However, OPV technology would also benefit from the introduction of non-fullerene acceptors. Unfortunately, efforts to replace fullerenes have typically led to significantly reduced efficiencies. A number of possible explanations for reduced efficiencies with non-fullerene acceptors compared to fullerene acceptors have been suggested, including the formation of unfavorable morphologies in non-fullerene systems and/or favorable excitation/carrier delocalization in fullerenes. In addition, enhanced exciton dissociation associated with fundamental characteristics of the fullerene molecular electronic states has also been suggested. We used time-resolved two-photon photoemission (TR-2PPE) to directly compare exciton dissociation at interfaces between zinc phthalocyanine (ZnPc) interfaces and the non-fullerene acceptor, perylene tetracarboxylic dianhydride (PTCDA) versus dissociation measured at the analogous interface with C_{60}, and thus help discriminate between these potential explanations. Exciton dissociation rates are comparable for phthalocyanine interfaces with both acceptors, allowing us to suggest a hierarchy for the importance of various effects producing higher efficiencies with fullerene acceptors.

* National Institute of Standards and Technology, 100 Bureau Dr., Gaithersburg, MD 20899
(301) 975-2550, steven.robey@nist.gov

Keywords: organic, photovoltaic, donor-acceptor, charge transfer, ultrafast, photoemission

I. Introduction

Significant progress has been made towards achieving viable device efficiencies for polymer and small molecule organic photovoltaics (OPV) over the past ≈ 5 years with power conversion efficiencies of 7 % now routine, and reaching 10 % and above for tandem structures.[1-7] The increase in efficiency has been driven by improved fundamental understanding of interfacial charge separation, electron and hole transport, and the role of morphology in OPV structures. This improved understanding has fueled the development of new donor organic materials that provide better optical absorption and carrier transport, as well as providing improved matching of the donor electronic energy levels- the highest occupied molecular orbitals (HOMO) and lowest unoccupied molecular orbitals (LUMO) - to (predominantly) fullerene-based acceptors.[8-10]

In contrast, investigation of the potential for improvement with the introduction of new n-type, acceptor small molecules and polymers has been more restricted.[11-15] Fullerenes and fullerene derivatives, such as [6,6]-phenyl-C_{61}-butyric acid methyl ester ($PC_{61}BM$) and [6,6]-phenyl-C_{71}-butyric acid methyl ester ($PC_{71}BM$) are very good electron acceptors and typically form nanoscale morphologies that promote high carrier mobility. However, an OPV technology based exclusively on fullerene acceptors is limited by the lack of ability to tune the fullerene LUMO level significantly and the poor absorption in the visible spectral range, limiting exciton generation predominantly to the donor material. The reliance on fullerenes also reduces the potential of OPV as a green and sustainable energy technology.[16] Fullerenes have high production costs, with estimates for the embodied energy (the sum of the energy associated with material production) several orders of magnitude larger for fullerenes than for the typical polymer or small molecule materials used as donors.[17,18] It has been suggested that the use of

fullerenes contributes 18 % to 30 % of the cumulative energy required for production in OPV technologies.[18] Thus, understanding the factors limiting the performance with non-fullerene acceptors may result in significant long-term benefits.

Molecular and polymeric materials based on perylene cores provide one potential class of alternate organic acceptors.[11-14,19-22] In fact, the first organic bilayer photovoltaic cell consisted of a phthalocyanine donor and a perylene tetracarboxylic dianhydride (PTCDA) acceptor.[23] Perylene-core compounds typically have low-lying LUMO levels and can be easily modified synthetically to tune the electronic structure and to control morphology, allowing optimization of molecular packing and electron transport. Perylene-based materials also exhibit increased optical absorption in the visible portion of the spectrum compared to fullerenes.

These characteristics have motivated interest in perylene-based acceptors for organic photovoltaic structures, but attempts to incorporate them in OPV structures have typically resulted in reduced efficiencies. The relatively poor performance of perylene-based acceptors has been attributed to several possible factors. The rigid, planar perylene core exhibits a tendency to produce large scale aggregation and crystallization, sometimes on the scale of microns, with concomitant phase separation and loss of intimate contact with the donor. Large-scale aggregation can thus result in reduced efficiency in bulk heterojunction structures due to poor exciton harvesting.[14,19-22] A second explanation for the disparity in performance is improved charge separation, following interfacial exciton dissociation, for fullerene-based systems compared to non-fullerene acceptors. Improved charge separation arises from more effective carrier delocalization in the C_{60} nano-aggregates and crystalline regions typically observed in well-performing bulk heterojunction blends based on fullerenes.[24-33]

Finally, fullerenes may have advantages due to their exceptional electron-accepting characteristics, associated with small reorganization energies and high degeneracies.[34-38] In this case, higher efficiencies arise from fundamentally increased rates of exciton dissociation at the donor-acceptor interface associated with the fullerene molecular electronic structure. Theoretical investigations comparing fullerene and non-fullerene acceptors found that multiple, stable low-lying excited states of the fullerene anion, and a selection of the other non-fullerene acceptors, may increase dissociation rates by orders of magnitude. Analogous stable excited states are absent in perylene-based molecules, such as PTCDA. [36, 37]

Previous studies of non-fullerene acceptors examined charge separation dynamics in OPV structures with perylene-based acceptors, using ultrafast vibrational spectroscopy[39] and transient absorption.[40] Vibrational spectroscopy was employed to monitor time-dependent shifts of the carbonyl vibrations associated with the fullerene acceptor, phenyl-C_{61}-butyric acid methyl ester (PCBM), or perylene diimide (PDI) derivative acceptors, providing clues to the long-range charge separation following exciton dissociation at the interface with poly(3-hexylthiophene) (P3HT). Significantly different temperature-dependent behavior observed for the two classes of acceptor led to the conclusion that, unlike the perylene-based acceptor, charge separation in the fullerene was nearly barrierless, consistent with enhanced delocalization in the PCBM phase.

Visible to near-infrared transient absorption measurements performed on bulk heterojunction structures formed with a low bandgap donor polymer and a PDI derivative acceptor led to two main conclusions. First, a large fraction (55 %) of the excitons generated in the donor polymer recombined without undergoing dissociation. This could signal either inefficient exciton harvesting, consistent with large-scale aggregation of the perylene acceptor, or inefficient

exciton dissociation at the interface. Second, of the exciton population that did undergo dissociation to a charge transfer state (45 % of the initial population), ≈ 40 % of these subsequently recombined geminately. This observation is also consistent with inefficient long-range charge separation from the CT state formed at the PDI acceptor interface.

Recent efforts based on designing molecules to overcome possible deficiencies of non-fullerene acceptors resulted in notable improvements with efficiencies reaching 5 % to 6 %,[41, 42] However, despite this success and fundamental studies of charge separation, the relative importance of (1) aggregation in non-fullerene acceptors versus (2) better charge separation due to delocalization in fullerenes versus (3) enhanced exciton dissociation via the fullerene molecular excited states remains unknown. To help discriminate between these factors, we directly compared exciton dissociation at phthalocyanine (Pc) interfaces with (C_{60}) and a non-fullerene acceptor (PTCDA) using time-resolved two-photon photoemission (TR-2PPE). PTCDA was chosen because it does not have the requisite set of low-lying excited states needed to induce enhanced exciton dissociation (factor (3) above).[36, 37] The focus of this work is thus to examine the potential for enhanced exciton dissociation with C_{60}, due to molecular electronic characteristics, compared to PTCDA.

TR-2PPE proved useful in a number of investigations of electronic structure and exciton dynamics at molecular donor-acceptor interfaces of interest for OPV.[43-51] The extreme surface sensitivity of TR-2PPE allows, when coupled with well-controlled formation of interfaces using organic molecular beam epitaxy (OMBE), isolation of the interface response and provides a means to directly measure exciton dissociation at the donor-acceptor interface.[49-51] For Pc/C_{60} heterojunctions, the decay rate of Pc S_1 excitons created by optical pumping at the Pc/C_{60} interface was compared with the decay in the bulk, allowing the rate of interfacial exciton

dissociation to be extracted.[50,51] In the work reported below, analogous measurements were performed for Pc/PTCDA interfaces to provide a comparison of the relative rates of exciton dissociation using PTCDA versus C_{60} acceptors.

We begin with a description of experimental methods and characterization of the donor-acceptor heterojunction structures, including determination of the interfacial electronic band alignment. The results of TR-2PPE measurements are then presented and discussed. Comparison of these results for ZnPc/PTCDA interfaces and previous investigations of C_{60}/H_2Pc structures reveals that exciton dissociation at the Pc/PTCDA interface is found to be comparable to dissociation at Pc/C_{60} interfaces. We end by discussing the implication this result may have in assessing the impact of possible factors driving higher OPV efficiencies with fullerene acceptors.

II. Experimental Methods

II(a). ZnPc\PTCDA bilayer formation

The sample structures used for TR-2PPE measurements are illustrated in Figure 1. These heterolayer structures were formed in ultrahigh vacuum (UHV) using organic molecular beam epitaxy (OMBE). The initial Ag(111) substrate was prepared by cycles of Ar^+ ion sputtering and annealing. A clean, well-ordered surface was verified both by work function and surface state linewidth as measured by He(I) ultraviolet photoemission spectroscopy (UPS) and the n = 1 image state binding energy measured with 2PPE.

A fullerene film, typically 5 layers, was grown on the clean Ag(111) prior to formation of the ZnPc/PTCDA heterjunctions. C_{60} deposition on Ag(111) leads to good layer-by-layer growth with nearly single-crystal films.[52-54] This spacer layer thus served to provide increased separation between the metal surface and the subsequently formed ZnPc/PTCDA interface,

blocking photoemission from the Ag(111) substrate,[50,51] without introducing significant roughness. We also expect this spacer layer to template good PTCDA crystalline films with nearly upright molecular orientation (molecular plane perpendicular to the surface/interface plane) as observed for the deposition on graphite.[55] In contrast, PTCDA deposition directly on metal surfaces typically leads to Stranski-Krastanov growth modes with three-dimensional island formation with increased thickness.[56] Photoemission from the fullerene layer had no impact on TR-2PPE measurements for the ZnPc/PTCDA interfacial region due attenuation by the thick PTCDA overlayers.[50]

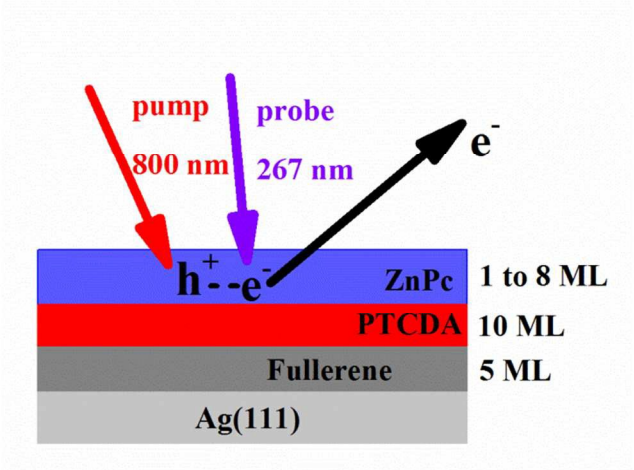

Figure 1 Layer structure used for TR-2PPE measurements. The pump-probe excitation scheme used for TR-2PPE is also illustrated in the figure.

PTCDA was deposited on the fullerene film from a separate effusion cell to a coverage of approximately 10 monolayers (ML) PTCDA, with the substrate maintained at room temperature. We define 1 ML PTCDA as the coverage resulting in complete attenuation of the UPS signal from the underlying fullerene layers. The PTCDA deposition was continued well beyond complete attenuation of C_{60} photoemission intensity and beyond the point where the photoemission features saturated to bulk PTCDA.

To form the ZnPc/PTCDA interface, variable thicknesses of ZnPc were deposited at room temperature on the PTCDA acceptor layer. Again, one ML was defined based on the attenuation of PTDCA photoemission features and was consistent with quartz crystal microbalance measurements of the ZnPc deposition rate. The initial attenuation of photoemission from the underlying PTCDA showed initial linear behavior with ZnPc deposition time, consistent with good ZnPc layer growth without significant three-dimensional islanding. With this protocol, the time-dependence of the structure monitored by TR-2PPE was independent of the PTCDA thickness, verifying that the fullerene sub-layers did not impact the measured dynamics of the ZnPc/PTCDA interface region. The rapid loss of PTCDA photoemission with ZnPc deposition is also consistent with previous studies that revealed that the photoemission intensity from the exciton population in the outermost Pc layers dominated the TR-2PPE measurements.[43,49-51]

II(b). UPS and Time-Resolved Two-Photon Photoemission

One- and two-photon photoemission data were collected with a hemispherical analyzer providing energy resolutions of 100 meV and 60 meV, respectively. A helium discharge lamp was the excitation source for UPS. For TR-2PPE, a Ti:sapphire oscillator (KMLabs Griffin, 35 fs, 80 MHz, 700 to 900 nm) provided ultrashort pulses.[57] The excitation sequence used for TR-2PPE is also illustrated in Figure 1. The Ti:sapphire fundamental at 800 nm ($h\nu_{pump}$ = 1.55 eV) was used to excite $\pi \rightarrow \pi^*$ Q band transitions from the ZnPc HOMO, populating ZnPc S_1 exciton levels. The third harmonic at 267 nm ($h\nu_{probe}$ = 4.65 eV) was then used to probe the dynamics of this population at variable delays. The pump and probe beams were focused to a diameter of ~100 μm, yielding a peak pump power density below 0.1 GW cm^{-2}. The probe power density was between 1 to 2 orders of magnitude lower. The pump and probe beams were

non-collinearly overlapped at the sample with perpendicular polarizations (s-pump, p-probe) to eliminate contributions from coherent two-color photoemission and isolate the dynamics of real intermediate states.

The work functions for these organic layer systems were determined by the mid-point of the photoemission threshold. The uncertainties represent one standard deviation over multiple measurements. The work function values varied from 4.5 ± 0.05 eV for the starting PTCDA surface to 4.1 ± 0.05 eV for the thickest (bulk) ZnPc films. The pump-probe sequence was sufficient to produce excitations into the ZnPc Q-band, and subsequently photoexcite from these states above the vacuum level, but also maintain the one-photon photoemission background excited with the UV probe at a manageable level.

Control TR-2PPE measurements were performed on neat ZnPc and PTCDA films. Pump-induced excitations from the ZnPc HOMO to S_1 excitons were observed for thick ZnPc samples, but no measurable pump response was observed for pure PTCDA. Absorption in PTCDA is significant only above ≈ 600 nm (2 eV). Also, the pump-probe combination employed here cannot induce photoemission from the PTCDA HOMO binding energy (≈ 1.5 eV deeper than the ZnPc HOMO) to final state energies above the sample work function.

TR-2PPE spectra were acquired at fixed pump-probe delay values ranging from $\Delta t = 0$ fs to $\Delta t = 200$ ps. Background spectra, obtained either with the probe pulse arriving before the pump or with the probe beam alone, were also acquired. The difference spectra produced by subtracting these background spectra from pump-plus-probe spectra were equivalent and were employed to isolate the pump-induced response. Probe-only spectra were also used to monitor and normalize the spectra for laser intensity variations. Cross-correlation (CC) measurements of the photoemission intensity as a function of pump-probe delay (from -0.5 ps to 250 ps) were

acquired at specific energies across the spectra. Additional detail on the TR-2PPE measurements is provided in Refs. 49-51.

III. Results and Discussion

III(a). Interfacial electronic structure

UPS spectra of samples with varying thicknesses of ZnPc on PTCDA are provided in Figure 2, along with a spectrum representing the starting PTCDA layer. In this initial spectrum, the PTCDA highest occupied molecular orbital (HOMO) is observed at 2.65 eV ± 0.05 eV. (Very weak structure at $E_b \approx -0.8$ eV is evident due to He(I) satellites). With deposition of ZnPc, the PTCDA HOMO is attenuated while the phthalocyanine HOMO at 1.50 ± 0.05 eV eV increases. For the smallest ZnPc deposition (labeled "sub-ML" ZnPc), structure from the underlying PTCDA HOMO is still weakly visible, consistent with an incomplete surface coverage. For the sample labeled "ML" ZnPc, deposition was continued just beyond the point where attenuation of PTCDA signal was complete and the ZnPc HOMO dominates the spectrum at low binding energy. The HOMO offset at this interface (threshold-to-threshold) is 1.0 eV ± 0.07 eV. The final spectrum of Figure 2 represents a nominal thickness of 8 ML ZnPc, and the UPS spectrum is consistent with a thick, bulk-like ZnPc film.

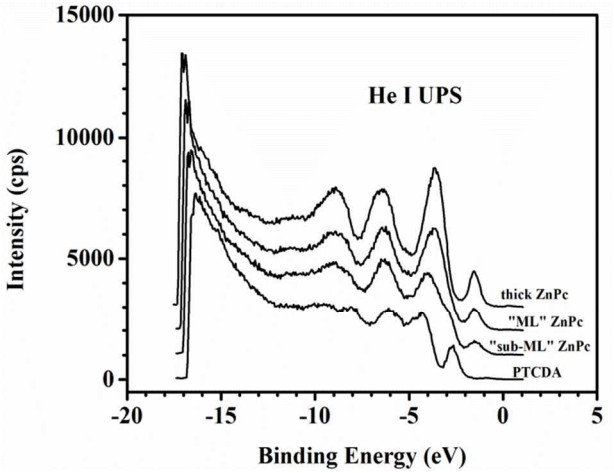

Figure 2 He I (21.2 eV) ultraviolet photoemission spectra for increasing coverage of ZnPc on PTCDA. The spectra are plotted versus the binding energy from the Fermi level, E_F, at 0 eV and are offset vertically for clarity. (See text for details.)

The interfacial band alignments at the two interfaces were determined based on combined UPS and 2PPE data from this work, published inverse photoemission (IPES)[58,59] and optical absorption data. This combination of measurements leads to the band diagram in Figure 3a for the ZnPc/PTCDA interface, compared with results from Refs. 49 and 50 for Pc/C_{60} interfaces in Figure 3b, providing the donor and acceptor HOMO, LUMO, and S_1 energy levels. Excitations (S_1, CT) are included in this single-particle diagram with the hole in the donor HOMO level.[60] The charge transfer (CT) states were estimated as the Pc-HOMO-to-acceptor-LUMO separation (threshold-to-threshold) minus the CT exciton binding energy. The CT levels are indicated in Figure 3 by the grey shaded regions. Comparable charge transfer exciton binding energies of ≈ 200 meV[61-63] were assumed for both interfaces.

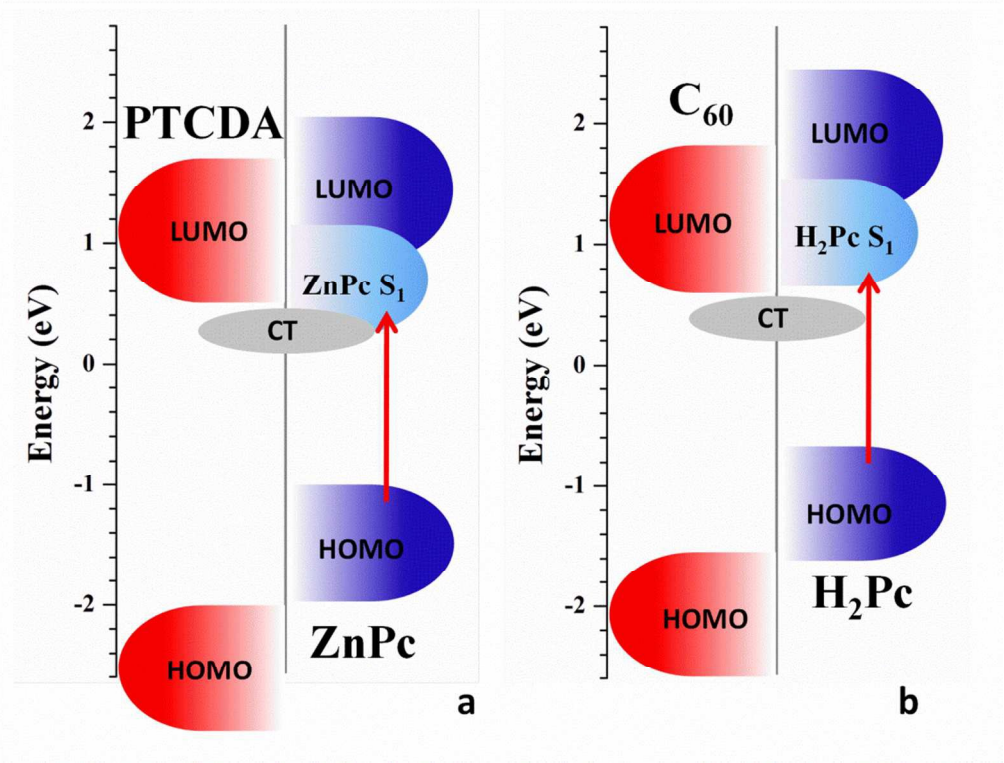

Figure 3 Interfacial electronic band alignments determined from UPS, IPES, and 2PPE are presented in a one-electron orbital/level representation for (a) the ZnPc/PTCDA interface and (b) the H_2Pc/C_{60} interface. The energy scale is referenced to the Fermi level, E_F, in both cases. The acceptor levels (HOMO, LUMO) are shown on the left (red) and the donor levels are on the right (blue) in each diagram. Locations for optical absorption to Pc S_1 levels are also provided, based on optical absorption, along with estimated positions for interfacial charge transfer states (CT) (see text).

From Figure 3, we conclude that the two acceptors have similar interfacial LUMO energy positions (relative to E_F) but a smaller (by ≈ 200 meV) Pc HOMO binding energy for Pc/C_{60} interfaces compared to Pc/PTCDA. A consequence of this lower lying Pc HOMO level for Pc/PTCDA interface is thus, with identical pump energies, excitations to the Pc S_1 levels have less excess energy above interfacial CT states at the Pc/PTCDA interface than at the interface with C_{60}. The potential impact of this difference will be discussed below.

III(b). TR-2PPE measurements

TR-2PPE measurements were performed for bulk-like ZnPc films ("thick ZnPc" in Figure 2) and for samples illustrated by the "sub-ML" case in Figure 2, where the coverage of ZnPc was incomplete. Measurements with this "sub-ML" case ensured that TR-2PPE monitored exciton dynamics for ZnPc molecules in intimate contact with the PTCDA acceptor layer (no significant 2nd ZnPc layer). The resulting TR-2PPE difference spectra are provided in Figure 4a for bulk ZnPc ("thick ZnPc" in Figure 2) and the interfacial region ("sub-ML" spectrum in Figure 2) in Figure 4b. The TR-2PPE spectra are plotted versus the final state kinetic energy, above the vacuum level. For each ZnPc thickness, spectra acquired at two pump-probe delays, $\Delta t = 0$ fs (black, solid symbols) and $\Delta t = 1$ ps (red, open symbols), are included in the figures. Analogous spectra for H_2Pc with C_{60} (Figure 4c, 1 ML H_2Pc/C_{60}) and thick H_2Pc/C_{60} heterolayers (Figure 4d) from Ref. 51 are also provided. (The peaks at low energy in the H_2Pc/C_{60} data are due to small pump-induced shifts between the pump-plus-probe spectra and the probe-only spectra used for background subtraction. This results in a shift of the background spectra and a peak in the difference. These shifts have essentially no impact on difference spectra in the S_1 intensity region above ≈ 0.3 eV where the background is essentially constant.)

The previous TR-2PPE studies of Pc/C_{60} interfaces [50,51] revealed that the pump-induced intensity in Figures 4c and 4d for the H_2Pc layers, and Figures 4a and 4b for ZnPc/PTCDA, arises from optical excitation of the Pc Q-band creating an optical transition from the H_2Pc HOMO to the H_2Pc LUMO. The differences in the spectral shape between the two systems is explained by the larger ZnPc HOMO binding energy on PTCDA (≈ 200 meV), producing

correspondingly reduced final state energies and increased truncation at the low energy work function threshold.

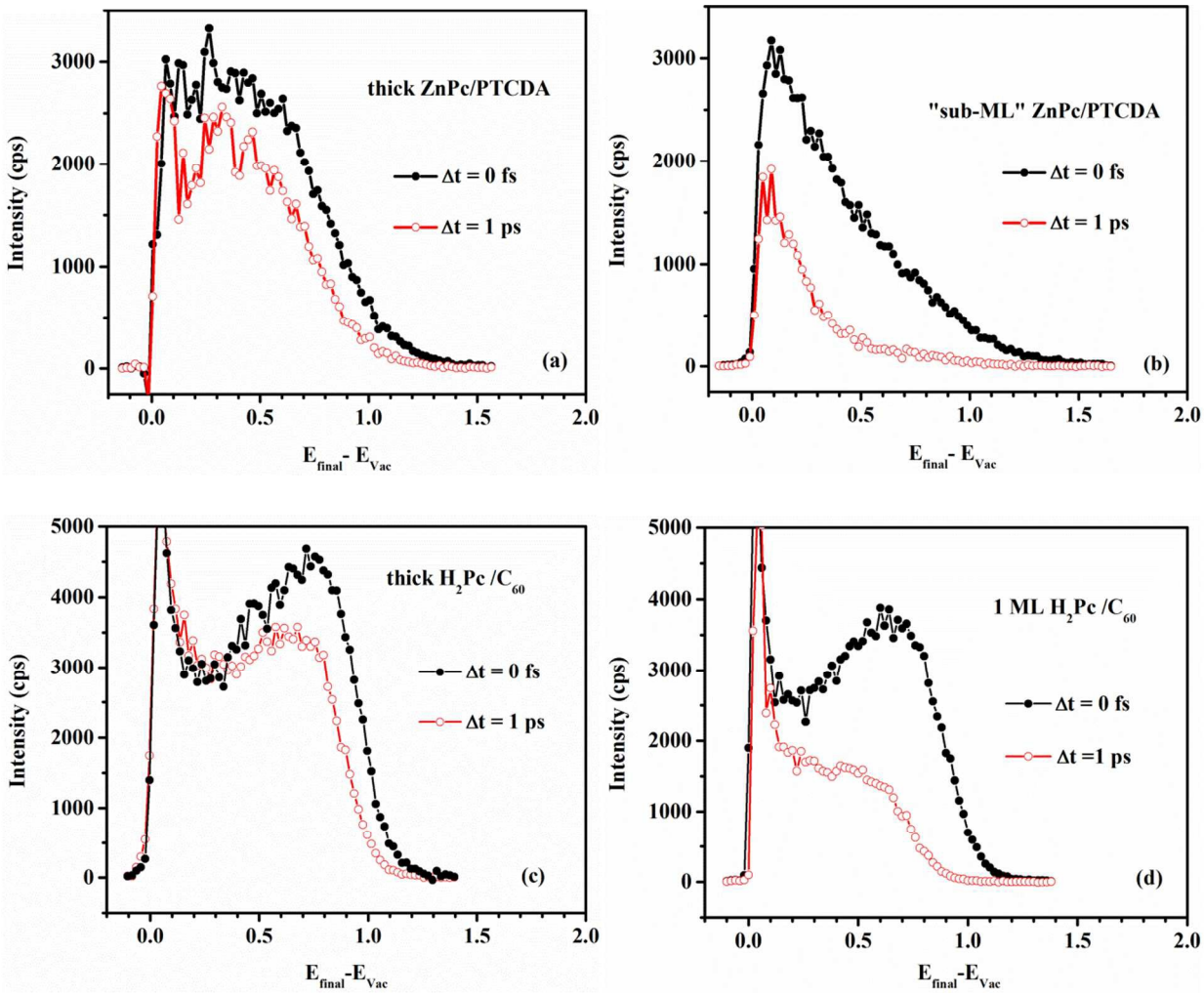

Figure 4 Comparisons of TR-2PPE spectra acquired with pump-probe delays of $\Delta t = 0$ fs and $\Delta t = 1$ ps for (a) a thick ZnPc layer on PTCDA, (b) a partial coverage of ZnPc on the PTCDA layer, "sub-ML" case from Figure 2, (c) a thick H_2Pc layer on C_{60}, and (d) a ML coverage of H_2Pc on C_{60}. (Figures (c) and (d) are from the study reported in Ref. 51.)

The loss of S_1 population between $\Delta t = 0$ fs and $\Delta t = 1$ ps for each heterolayer structure is revealed by the change in intensity between the pairs of spectra, black versus red, in each of the figures. Comparing Figure 4a and Figure 4b, the loss of population in the first ps clearly larger for the interfacial layer ("sub-ML" sample, Figure 4b) compared to the thick (bulk) ZnPc case (Figure 4a). The same increased decay at the interface is also evident in the data for H_2Pc/C_{60} in

Figure 4c and Figure 4d. This more rapid loss of population at the interface in both cases arises from exciton dissociation.[50,51]

A simple qualitative examination of the data in Figure 4 suggests that increased in population decay for the interfacial donor Pc layers, due to exciton dissociation, is similar for both donor-acceptor pairs. The loss of S_1 intensity within the first picosecond for the spectrum representing the ZnPc/PTCDA interface is about 70 % and about 60 % for the analogous H_2Pc/C_{60} spectrum. Some loss of S_1 intensity in the corresponding thick films occurs primarily due to relaxation of the S_1 population to lower energy out of the experimentally accessible photoemission window (limited by the work function). If this is subtracted from the population loss observed noted above for the interfacial layers, the loss due to exciton dissociation is estimated to be about 42 % for ZnPc/PTCDA and 38 % for H_2Pc/C_{60}, suggesting similar exciton dissociation efficiencies for both acceptor interfaces.

The CC data provide a more quantitative time-resolved picture of the decay dynamics. CC measurements for two of the ZnPc/PTCDA samples represented in Figure 4 are displayed in Figure 5. Figure 5a provides the CC data for delays to 1 ps and Figure 5b provides the same data to 500 fs in a log-linear format (black curves in each figure). The data in this figure were obtained by averaging CC curves acquired in the high energy portion of the spectra in Figures 4a and 4b, from E_{final}- E_{vac} = 0.8 eV to 1.0 eV. The CC data in this energy range exhibit the greatest sensitivity to interfacial dissociation and charge transfer because overlap with lower energy relaxed states is excluded.[51] The gray dashed curve in each of the figures represents the experimental time resolution function obtained by measuring the pump-probe cross correlation for the Ag(111) surface state giving a full-width at half-maximum of 160 fs ± 10 fs. (The cross-correlation width is larger than the oscillator pulse width of 35 fs largely due to pulse broadening

in the harmonic generation step.) CC data for the H_2Pc/C_{60} system with 1 ML H_2Pc and a thick H_2Pc layer (blue curves) are also included in Figures 5a and 5b for comparison.

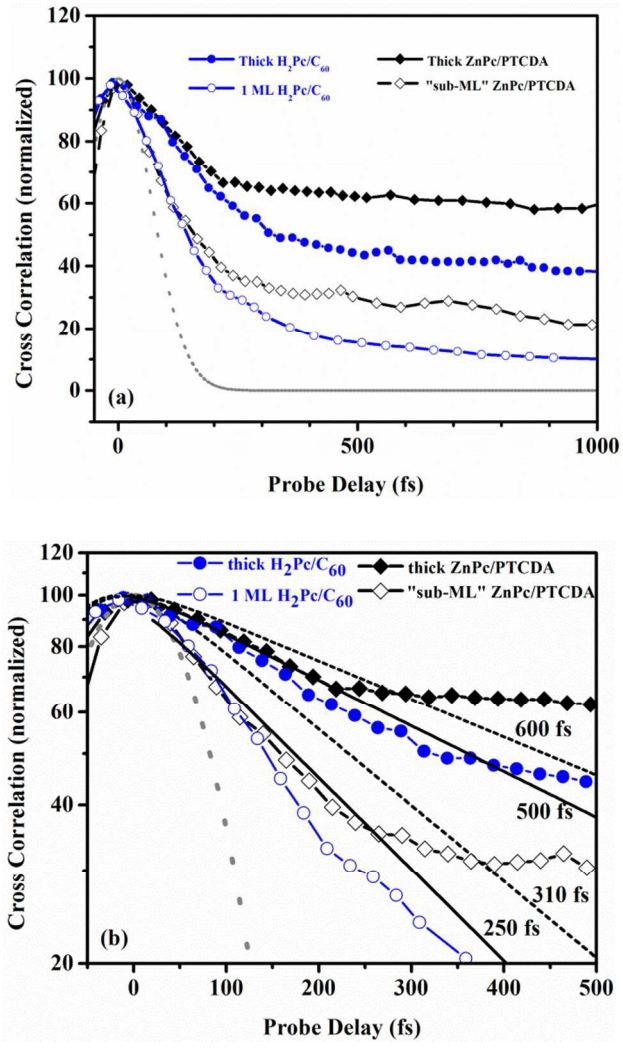

Figure 5 Pump-probe cross-correlation (CC) curves representing the decay of the Pc S_1 population with time are provided for two ZnPc/PTCDA interface cases ("sub-ML" and thick ZnPc, black data) and for H_2Pc/C_{60} interfaces from Ref. 51 (1 ML and thick H_2Pc, blue data). The data are plotted for delays up to 1 ps in (a) and up to delays of 500 fs in (b) in a ln-linear format. The curves were normalized at $\Delta t = 0$ probe delay. In Figure 5a the dashed black lines represent model fits (convolution of the experimental resolution function - dashed gray line - with exponential functions) over the complete delay range to 500 fs. The solid lines are fits over only the linear region of the CC data at small delay. The resulting values for τ are provided alongside the fits. The fits are to the ZnPc/PTCDA data (black) only. The H_2Pc/C_{60} data (blue) are included only for comparison.

The CC data were analyzed using a rate equation model,

$$\frac{dN_{S_1}}{dt} = I_0\, I_{pump}(t) - N_{S_1}(t)/\tau. \qquad (1)$$

N_{S_1}(t) is the S_1 population as a function of time, I_0 is the (assumed constant) transition rate at the pump energy, $I_{pump}(t)$ is the instantaneous pump-pulse intensity, and τ is the decay lifetime (The decay rate constant is given by 1/τ.). Assuming that bulk relaxation processes governing the decays for thick films do not change significantly near the interface, then the rate of exciton dissociation at the interface is given by the difference between the decay rates for the thick and thin film cases.[50]

Based on this model, the CC data were fit to the convolution of the experimental resolution function with the exponential decay, represented by τ. This analysis is appropriate for kinetics slower than the experimental resolution. Fits to the ZnPc data were performed over different ranges starting at 50 fs and ending with various delays to a maximum of 500 fs. The best fit value for the "sub-ML" ZnPc/PTCDA interface data was τ(sub-ML) = 310 fs ± 50 fs, but a value of 250 fs resulted if the range was restricted to the linear region of the CC data at small delay. Fitting the thick ZnPc/PTCDA data over the full range to a delay of 500 fs resulted in τ (Thick) = 600 fs ± 90 fs while fitting over the region of small delays resulted in a lifetime of 500 fs. Example fits using the full delay range to 500 fs are provided in Figure 5 as dashed lines and the best fits at small delays are given as solid lines. The spread in τ as a function of the fitting range, arising from increased non-linearity/change-in-slope at larger delay, is the primary source of the uncertainties. Multi-exponential fits were also performed to assess the impact of slower decays for pump-probe delays > 500 fs (not shown). This modified the decay constants by less than 5%, within the stated uncertainties, and had no impact on the resulting comparison between C_{60} and PTCDA.

For the H_2Pc/C_{60} interface, the rate of interfacial exciton dissociation was determined previously to be $k_{CT} = (2.3 \pm 0.4) \times 10^{12}$ s^{-1}. [50] For the ZnPc/PTCDA interface, the result is

k_{CT} = 1/(310 fs) - 1/(550 fs) = 3.2 x 10^{12} s^{-1} - 1.8 x 10^{12} s^{-1} = 1.4 x 10^{12} s^{-1}, only slightly smaller than the rate with the fullerene acceptor, with an uncertainty in k_{CT} given by ± 0.5 x 10^{12} s^{-1}. When the analysis is restricted to the linear portion of the CC decays $k_{CT} \approx 2 \times 10^{12}$ s^{-1}. These quantitative results are thus consistent with the estimate above, suggesting again that the rate for exciton dissociation is comparable with both acceptors. We note that the measured values of k_{CT} are not limited significantly by the experimental time resolution (grey dashed line in Figure 5).

IV. Implications for higher efficiency with fullerene acceptors

Several potential explanations for the higher efficiencies observed with fullerene acceptors in OPV structures were noted in the Introduction, including (1) increased aggregation in non-fullerene acceptors; (2) increased charge and/or exciton delocalization in fullerenes, leading to better charge separation and; (3) increased exciton dissociation associated with the fullerene molecular excited states and/or low reorganization energies in fullerenes. Building on the TR-2PPE results provided above, we will now examine to what extent these help limit the possible explanations. In particular, the following discussion examines how the observation of comparable exciton dissociation at Pc interfaces with both C_{60} and PTCDA acceptors might or might not be reconciled with exciton dissociation that is larger for fullerenes (by orders of magnitude) due to fundamental molecular characteristics.[34-38]

The TR-2PPE measurements are not sensitive to the effects associated with aggregation ((1) above) in the perelyene-based acceptor, PTCDA. Increased aggregation in the acceptor would lead to decreased exciton harvesting prior to a measurement of dissociation at the interface [14,19,20] so these results cannot provide any indication of the effect of aggregation for fullerene versus non-fullerene acceptors.

Increased delocalization of exciton or carrier states can impact separation of charges from initially bound CT states and may also impact the effectiveness, and range, of dissociation due to the large, delocalized acceptor-state manifold.[64-66] As already noted, C_{60} layers grown by OMBE on Ag(111) are nearly single-crystal quality.[52-54] The donor-C_{60} interface is optimal from the point of view of delocalization in C_{60} and should aid increased efficiency for exciton dissociation with C_{60}, complementing effects associated with C_{60} molecular electronic structure. Poor delocalization thus cannot be used to rationalize a rate comparable with PTCDA.

Differences in the electronic structure for the Pc/C_{60} and Pc/PTCDA interfaces noted above could also impact the relative efficiency for exciton dissociation. However, the measured band alignments for the Pc/C_{60} and Pc/PTCDA interfaces revealed that the band offset, which may impact the excess energy available for exciton dissociation, is more favorable at the Pc/C_{60} interface. Again, this should produce increased exciton dissociation with the fullerene, above any possible advantages associated with C_{60} molecular characteristics.[36,37]

Finally, the relative molecular orientation of the donor and acceptor at the interface can also impact interfacial exciton dissociation probabilities. For Pc/C_{60} interfaces, scanning tunneling microscopy revealed that the Pc molecules were arranged with the molecular plane nearly perpendicular to the interface, with an estimated angle > 70 ° between the plane of the Pc molecule and the Pc/C_{60} interface.[50,53,67] However, the detailed molecular structure at the Pc/PTCDA interfaces is not known. As noted above, we suspect an orientation with the PTCDA molecular plane close to perpendicular to the interface with C_{60} and the pi-stacking direction along the surface/interface.[55,56] Weak interactions between Pc and PTCDA on this surface would then also likely result in Pc π-π stacking along the interface, possibly producing a relative orientation with both PTCDA and Pc molecular planes nearly perpendicular to the interface.

This relative orientation could be expected to lead to poor coupling for this interface as well but we can only speculate on this point currently.

We can instead attempt to estimate the magnitude of potential effects associated with molecular orientation based on a recent study of ZnPc/C_{60} interfaces with different relative orientations.[68] The short-circuit current, J_{SC}, was found to increase by a factor of about 50 % for interfaces with the ZnPc molecular plane nearly parallel to the interface (face-on), compared to the nearly perpendicular (edge-on) orientation. The authors concluded that the primary origin of the increase in J_{SC} was improved exciton dissociation for the "face-on" ZnPc/C_{60} interface. Complementary calculations of the effective electronic couplings, V_{eff}, and exciton dissociation rates, $k_{CT} \sim V_{eff}^{2}$, suggested an increase of k_{CT} by $\geq$ 30 % for face-on interface orientations, consistent with the experimental findings. The TR-2PPE data provided in Figures 4 and 5 correspond to an interface with a predominantly "edge-on" orientation of the Pc molecule and thus, based on Ref. 68, might be expected to exhibit reduced exciton dissociation efficiency compared to an "optimum" interface with a "face-on" orientation, by ≈ 50 %.

"Core-clock" resonant auger electron spectroscopy methods were also used to measure the electron transfer rates of core-π* excitons at Pc/C_{60} interfaces as a function of the relative orientation of the CuPc ("edge-on" versus "face-on").[69]. These data also suggested increased rates for "face-on" Pc/C_{60} orientations, compared to "edge-on". The magnitude of the relative increase varied with the analysis energy within the N(1s) absorption region, from a factor of ≈ 1 (no change with orientation) to ≈ x 3.

To summarize, TR-2PPE measurements of interfacial exciton dissociation are not sensitive to any aggregation-induced reductions in exciton harvesting for perylene acceptors and thus cannot provide information on lower efficiencies compared to fullerenes due to potential explanation.

The effect of delocalization on exciton dissociation should be optimized for C_{60} at the Pc/C_{60} interfaces, due to the very well-ordered C_{60} layers used in the Pc/C_{60} studies, and interfacial band alignment should also be more favorable for Pc/C_{60} than Pc/PTCDA. Finally, although the orientation at this specific Pc/C_{60} interface is not optimal and could produce a reduction in exciton dissociation with C_{60}, the available experimental results suggest that the impact would be in the range of 50 % to, at most, a factor of 3.

The observation of similar rates of dissociation for the fullerene (C_{60}) and non-fullerene (PTCDA) acceptors with Pc donors is hard to reconcile with fundamentally much greater (orders of magnitude) dissociation rates for molecular C_{60}. Increased exciton dissociation with fullerenes evident in calculations [36] is not apparent in the experimental comparison. Enhanced dissociation associated with the acceptor excited state structure may be moderated by the complex heterogeneous solid state interfaces with, for instance, broadened manifolds of acceptor and donor states. Exciton dissociation in the Marcus inverted regime was highlighted in Ref. 36 as a key feature that leads to the enhanced dissociation for systems with high-lying excited acceptor states, such as fullerenes, compared to those without, such as PTCDA. The excitation conditions used for TR-2PPE produced low energy excitations in the Pc S_1 manifold, providing a reasonable representation of the relaxed exciton population reaching the DA interface via diffusion. Excitons at these energies are, however, close to the expected energy of CT states for these interfaces [49-51] so that, after relaxation, dissociation will not necessarily occur in the Marcus inverted regime. The potential for higher efficiencies in fullerene-based OPV driven by inherent molecular characteristics can thus be impacted by factors, such as structure (molecular and electronic) at the DA interface, which warrant further investigation. Although this effect may play a role in the dominance of high efficiency DA combinations with fullerenes, other

explanations based on carrier/charge transfer state delocalization, leading to efficient charge separation after dissociation,[24-33] and/or excessive aggregation/phase separation with perylene constituents,[14,19,20] may be as, or even more, important.

V. Summary

Time-resolved two-photon photoemission was employed to gauge the relative efficiency of exciton dissociation at the ZnPc/PTCDA interface compared to the rate measured at a Pc interface with the fullerene acceptor, C_{60}. The interfacial exciton dissociation rate at the ZnPc/PTCDA interface was $k_{CT} = (1.4 \pm 0.5) \times 10^{12}$ s^{-1}, based on the difference between the S_1 exciton population decay in the ZnPc layer adjacent to PTCDA compared with the decay far from the interface. This is comparable (within a factor of two) to the rate measured at the interface between H_2Pc and fullerene (C_{60}).[51] Other factors with potential impact on the relative rates of interfacial exciton dissociation for fullerene versus perylene-based acceptors, such as molecular orientation effects and/or differences in the interfacial electronic structure, were considered. Estimates of the potential impact of these factors, coupled with quantitatively similar rates of dissociation at both interfaces, lead to the conclusion that exciton dissociation is not greatly enhanced due to inherent features of the fullerene molecular electronic structure, implying that other factors such as the degree of aggregation/phase segregation and/or ability to enhance carrier delocalized states are of as much, or more, importance.

References

[1] X. Guo, M. Zhang, W. Ma, L. Ye, S. Zhang, S. Liu, H. Ade, F. Huang, and J. Hou, Enhanced Photovoltaic Performance by Modulating Surface Composition in Bulk Heterojunction Polymer Solar Cells Based on PBDTTT-C-T/$PC_{71}BM$, *Adv. Mater.*, 2014, **26**, 4043–4049.

[2] Heliatek: http://www.heliatek.com/, 2013.

[3] J. Zhou, Y. Zuo, X. Wan, G. Long, Q.Zhang, W. Ni, Y. Liu, Z. Li, G.He, C. Li, B. Kan, M. Li, and Y. Chen, Solution-Processed and High-Performance Organic Solar Cells Using Small Molecules with a Benzodithiophene Unit, *J. Am. Chem. Soc.*, 2013, **135**, 8484 -8487.

[4] Solarmer: http://www.solarmer.com/, 2011.

[5] Z. He, C. Zhong, S. Su, M. Xu, H. Wu, and Y. Cao, Enhanced Power-Conversion Efficiency in Polymer Solar Cells Using an Inverted Device Structure, *Nat. Photonics*, 2012, **6**, 591-595.

[6] You, J., Chen, C.-C., Hong, Z., Yoshimura, K., Ohya, K., Xu, R., Ye, S., Gao, J., Li, G. and Yang, Y. (2013), 10.2% Power Conversion Efficiency Polymer Tandem Solar Cells Consisting of Two Identical Sub-Cells. *Adv. Mater.*, **25**, 3973–3978.

[7] W. Li, A, Furlan, K. H. Hendriks, M. M. Wienk, and R. A. J. Janssen, Efficient Tandem and Triple-Junction Polymer Solar Cells, *J. Am. Chem. Soc.*, 2013, 135, 5529–5532.

[8] Y. Liang, D. Feng, Y. Wu, S.-T. Tsai, G. Li, C. Ray, and L. Yu, Highly Efficient Solar Cell Polymers via Fine-Tuning of Structural and Electronic Properties, *J. Am. Chem. Soc.*, 2009, **131**, 7792-7799.

[9] Y. Lin, Y. Li, and X. Zhan, Small Molecule Semiconductors for High-Efficiency Organic Photovoltaics, *Chem. Soc. Rev.*, 2012, 41, 4245-4272.

[10] Y. Liang and L. Yu, A New Class of Semiconducting Polymers for Bulk Heterojunction Solar Cells with Exceptionally High Performance, *Accts. Chem. Res.*, 2010, **43**, 1227-1236.

[11] P. Sonar, J. P. F. Lim, and K. L. Chan, Organic Non-Fullerene Acceptors for Organic Photovoltaics, *Energy Environ. Sci.*, 2011, **4**, 1558-1574.

[12] A. Facchetti, Polymer Donor-Polymer Acceptor (All-Polymer) Solar Cells, *Mats. Today*, 2012, 16, 123-132.

[13] Y. Kim and E. Lim, Development of Polymer Acceptors for Organic Photovoltaic Cells, *Polymers*, 2014, **6**, 382-407.

[14] A. F. Eftaiha, J.-P. Sun, I. G. Hill, and G. C. Welch, Recent Advances of Non-Fullerene, Small Molecular Acceptors for Solution Processed Bulk Heterjunction Solar Cells, *J. Mater. Chem. A*, 2014, **2**, 1201-1213.

[15] I. H. Jung, W.-Y. Lo, J. Jang, W. Chen, D. Zhao, E. S. Landry, L. Lu, D. V. Talapin, and L. Yu, Synthesis and Search for Design Principles of New Electron Accepting Polymers for All-Polymer Solar Cells, *Chem. Mater.*, 2014, **26**, 3450-3459.

[16] D. J. Burke and D. J. Lipomi, Green Chemistry for Organic Solar Cells, *Energy Environ. Sci.*, 2013, **6**, 2053-2066.

[17] A. Anctil, C. W. Babbitt, R. P. Raffaelle, and B. J. Landi, Material and Energy Intensity of Fullerene Production, *Environ. Sci. and Technol.*, 2011, **45**, 2353-2359.

[18] A. Anctil, C. W. Babbitt, R. P. Raffaelle, and B. J. Landi, Cumulative Energy Demand for Small Molecule and Polymer Photovoltaics, *Progress in Photovoltaics: Res. and Appl.*, 2013, **21**, 1541-1554.

[19] Q. Yan, Y. Zhou, Y.-Q. Zheng, J. Pei, and D. Zhao, Towards Rational Design of Organic Electron Acceptors for Photovoltaics: A Study Based on Perylenediimide Derivatives, *Chem. Sci.*, 2013, **4**, 4389-4394.

[20] R. Shivanna, S. Shoaee, S. Dimiitrov, S. K. Kandappa, S. Rajaram, J. R. Durrant, and K. S. Narayan, Charge Generation and Transport in Efficient Organic Bulk Heterojunction Solar Cells with a Perylene Acceptor, *Energy Environ. Sci.*, 2014, **7**, 435-441.

[21] S. Rajarman, R. Shivanna, S. K. Kandappa, and K. S. Narayan, Nonplanar Perylene Diimides as Potential Alternatives to Fullerenes in Organic Solar Cells, *J. Phys. Chem. Lett.*, 2012, **3**, 2405-2408.

[22] X. Zhang, Z. Lu, L. Ye, C. Zhan, J. Hou, S. Zhang, B. Jiang, Y. Zhao, J. Huang, S. Zhang, Y. Liu, Q. Shi, Y. Liu, and J. Yao, A Potential Perylene Diimide Dimer-Based Acceptor Material for Highly Efficient Solution-Processed Non-Fullerene Organic Solar Cells with 4.03% Efficiency, *Adv. Mater.*, 2013, **25**, 5791-5797.

[23] C. W. Tang, 2-Layer Organic Photovoltaic Cell, *Appl. Phys. Lett.* 1986, **48**, 183-185.

[24] S. D. Dimitrov and J. R. Durrant, Materials Design Considerations for Charge Generation in Organic Solar Cells, *Chem. Maters.*, 2014, **26**, 616-630.

[25] S. Gelinas, A. Rao, S. L. Smith, A. L Chin, J. Clark, T. S. van der Poll, G. C. Bazan, and R. H. Friend, Ultrafast Long-Range Charge Separation in Organic Semiconductor Photovoltaic Diodes, *Science*, 2014, **343**, 512-515.

[26] A. A. Bakulin, A. Rao, V. G. Pavelyev, P. H. M. van Loosdrecht, M. S. Pshenichnikov, D. Niedzialek, J. Cornil, D. Beljonne, and R. H. Friend, The Role of Driving Energy and Delocalized States for Charge Separation in Organic Semiconductors, *Science*, 2012, **335**, 1340-1344.

[27] B. Bernardo, D. Cheyns, B. Verreet, R. D. Schaller, B. P. Rand, and N. C. Giebink, Delocalization and Dielectric Screening of Charge Transfer States in Organic Photovoltaic Cells, *Nature Comm.*, 2014,

[28] B. M. Savoie, A. Rao, A. A. Bakulin, S. Gelinas, B. Movaghar, R. H. Friend, T. J. Marks, and M. A. Ratner, Unequal Partnership: Asymmetric Roles of Polymeric Donor and Fullerene Acceptor in Generating Free Charge, *J. Am. Chem. Soc.*, 2014, **136**, 2876-2844.

[29] H. Tamura and I. Burghardt, Ultrafast Charge Separation in Organic Photovoltaics Enhanced by Charge Delocalization and Vibronically Hot Exciton Dissociation, *J. Am. Chem. Soc.*, 2103, **135**, 16364-16367.

[30] A. Troisi, How Quasi-Free Holes and Electrons are Generated in Organic Photovoltaic Interfaces, *Faraday Discuss.*, 2013, **163**, 377-392.

[31] D. Veldman, O. Ipek, S. C. J. Meskers, J. Sweelssen, M. M. Koetse, S. C. Veenstra, J. M. Kroon, S. S. van Bavel, J. Loos, and R. A. J. Janssen, Compositional and Electric Field Dependence of the Dissociation of Charge Transfer Excitons in Alternating Polyfluorene Coploymer/Fullerene Blends, *J. Am. Chem. Soc.* 2008, **130**, 7721-7735.

[32] D. H. K. Murthy. M. Gao, M. J. W. Vermeulen, L. D. A. Siebbeles, and T. J. Savenije, Mechanism of Mobile Charge Carrier Generation in Blends of Conjugated Polymers abd Fullerenes: Significance of Charge Delocalization and Excess Energy, *J. Phys. Chem. C* 2012, **116**, 9214-9220.

[33] K. Vandewal, S. Albrecht, E. T. Hoke, K. R. Graham, J. Widmer, J. D. Douglas, M. Schubert, W. R. Mateker, J. T. Bloking, G.F. Burkhard, A. Sellinger, J. M. J. Fréchet, A. Amassian, M. K. Riede, M. D. McGehee, D. Neher, and A. Salleo, Efficient charge generation by relaxed charge-transfer states at organic interfaces, *Nature Maters.* 2013, **13**, 63-68.

[34] R. C. Haddon, The Fullerenes: Powerful Carbon-Based Electron Acceptors [and Discussion] *Philosophical Transaction of the Royal Society of London Series A- Mathematical Physical Engineering Sciences* 1993, **343**, 53-62.

[35] D. M. Guldi, Fullerenes: Three Dimensional Electron Acceptor Materials, *Chem. Commun.* 2000, 321-327.

[36] T. Liu and A. Troisi, What Makes Fullerene Acceptors Special as Electron Acceptors in Organic Solar Cells and How to Replace Them, *Adv. Mater.* 2013, **25**, 1038-1041.

[37] H. Ma and A. Troisi, Modulating the Exciton Dissociation Rate by More than Two Orders of Magnitude by Controlling the Alignment of LUMO+1 in Organic Photovoltaics, Organic Solar Cells and How to Replace Them, *J. Phys. Chem. C* 2014, **118**, 27272-27280.

[38] S. Klaiman, E. V. Gromov, and L. S. Cederbaum, All for One and One for All: Accommodating an Extra Electron in C_{60}, *Phys. Chem. Chem. Phys.*, 2014, **16**, 13287-13293.

[39] R. D. Pensack, C. Guo, K. Vakhshouri, E. D. Gomez, and J. B. Asbury, Influence of Acceptor Structure on Barriers to Charge Separation in Organic Photovoltaic Materials, *J. Phys. Chem. C* 2012**, 116**, 4824-4831.

[40] D. Gehrig, I. A. Howard, V. Kamm, C. Dyer-Smith, F. Etzold, and F. Laquai, Charge Generation in Polymer:Perylene Diimide Blends Probed by Vis-NIR Broadband Transient Absorption Pump-Probe Spectrsocopy, *Proc. of SPIE* 2013, **8811**, 88111F.

[41] Y. Zhong, M. T. Trinh, R. Chen, W. Wang, P. P. Khlyabich, B. Kumar, Q. Xu, C.-Y. Nam, M. Y. Sfeir, C. Black, M. L. Steigerwald, Y.-L. Loo, S. Xiao, F. Ng, X.-Y. Zhu, and C. Nuckolls, Efficient Organic Solar Cells with Helical Perylene Diimide Electron Acceptors, *J. Am. Chem. Soc.* 2014, **136**, 15215-15221.

[42] H. Li, T. Earmme, G. Ren, A. Saeki, S. Yoshikawa, N. M. Murari, S. Subramaniyan, M. J. Crane, S. Seki, and S. A. Jenekhe, Beyond Fullerenes: Design of Nonfullerene Acceptors for Efficient Organic, *J. Am. Chem. Soc.* 2014, **136**, 14589-14597.

[43] A. E. Jailaubekov, A. P Willard, J. R. Tritsch, W.-L. Chan, N. Sai, R. Gearba, L. G. Kaake, K. J. Williams, K. Leung, P. J. Rossky, and X. Y. Zhu, Hot Charge-Transfer Excitons Set the Time Limit for Charge Separation at Donor/Acceptor Interfaces in Organic Photovoltaics, *Nature Mater.* 2013, **12**, 66-73.

[44] J. R.Tritsch, W.-L. Chan, X. X. Wu, N. R. Monahan, X. Y. Zhu, Harvesting Singlet Fission for Solar Energy Conversion via Triplet Energy Transfer, *Nature Comm.* 2013, **4**, 2679.

[45] T. Wang and W.-L. Chan, Wai-Lun, Dynamical Localization Limiting the Coherent Transport Range of Excitons in Organic Crystals, *J. Phys. Chem. Letts.* 2014, **5**, 1812-1818.

[46] E. Varene and P. Tegeder, Polaron Dynamics in Thin Polythiophene Films Studied with Time-Resolved Photoemission, *Appl. Phys. A* 2012, **107**, 13-16.

[47] M. L. Blumenfeld, M. P. Steele, and O. L. A. Monti, Near- and Far-Field Effects on Moleucar Energy Level Alignment at an Organic/Electrode Interface, *J. Phys. Chem. Letts.* 2010, **1**, 145-148.

[48] B. W. Caplins, D. E. Suich, A. J. Shearer, and C. B. Harris, Metal/Phthalocyanine Hybrid Interface States on Ag(111), *J. Phys. Chem. Letts.* 2014, **5**, 1679-1684.

[49] G. J. Dutton, W. Jin, J. E. Reutt-Robey, S. W. Robey, Ultrafast Charge-Transfer Processes at an Oriented Phthalocyanine/C_{60} Interface, *Phys. Rev B* 2010, **82**, 073407(1-4).

[50] G. J. Dutton, S. W. Robey, Exciton Dynamics at CuPc/C_{60} Interfaces: Energy Dependence of Exciton Dissociation, *J. Phys. Chem. C* 2012**, 116**, 19173-19181.

[51] G. J. Dutton and S. W. Robey, Distance Dependence of Exciton Dissociation at a Phthalocyanine-C_{60} Interface, *J. Phys. Chem. C*, 2013, **48**, 25414-25423.

[52] Y. Yoshida, N. Tanigaki, and K. Yase, In Situ Observation of the In-plane Structure of C_{60} Thin Films on Metal Substrates Prepared by Moleuclar Beam Deposition, *Thin Solid Films* 1996, **281-282**, 80-83.

[53] W. Jin, Ph.D. Thesis, *Scanning Tunneling Microscopy / Spectroscopy Studies of Binary Organic Films*, University of Maryland, 2010.

[54] G. J. Dutton, D. B. Dougherty, W. Jin, J. E. Reutt-Robey, and S. W. Robey, Superatom Orbitals of C_{60} on Ag(111): Two-Photon Photoemission and Scanning Tunneling Spectroscopy, *Phys. Rev. B* 2011, **84**, 195435.

[55] C. Ludwig, B. Gomp, W. Glatz, J. Petersen, W. Eisenmenger, M. Mobus, U. Zimmermann, and N. Karl, Video-STM, LEED, and X-ray Diffraction Investigations of PTCDA on Graphite, *Z. Phys.-Cond. Matter* 1992, **86**, 397-404.

[56] G. Witte and C. Woll, Growth of Aromatic Molecules on Solid Substrates for Applications in Organic Electronics, *J. Mater. Res.* 2004, **19**, 1889-1916.

[57] Certain commercial equipment, instruments, or materials are identified in this paper to foster understanding. Such identification does not imply recommendation or endorsement by the National Institute of Standards and Technology, nor does it imply that the materials or equipment are necessarily the best available for this purpose.

[58] R. Hesper, L. H. Tjeng, and G. A. Sawatzky, Strongly Reduced Band Gap in a Correlated Insulator in Close Proximity to a Metal. *Europhys. Lett.* 1997**, 40**, 177-182.

[59] S. Krause, M. B. Casu, A. Scholl, and E. Umbach, E. Determination of Transport Levels of Organic Semiconductors by UPS and IPS. *New Journal of Physics* 2008, **10**, 085001(1-16).

[60] X.-Y. Zhu, How to Draw Energy Level Diagrams in Excitonic Solar Cells, *J. Phys. Chem. Letts.* 2014, **5**, 2283-2288.

[61] T. M. Clarke and J. R. Durrant, Charge Photogeneration in Organic Solar Cells. *Chem. Rev.* 2010, **110**, 6736-6767.

[62] R. H. Friend, M. Phillips, A. Rao, M. W. B. Wilson, Z. Li, C. R. McNeill, Excitons and Charges at Organic Semiconductor Heterojunctions. *Faraday Discuss.* 2012, **155**, 339–348.

[63] S. Gelinas, O. P. Labrosse, C.-N. Brosseau, S. Albert-Seifried, C. R. McNeill, K. R. Kirov, I. A. Howard, R. Leonelli, R. H. Friend, and C. Silva The Binding Energy of Charge-Transfer Excitons Localized at Polymeric Semiconductor Heterojunctions. *J. Phys. Chem. C* 2011, **115**, 7114–7119.

[64] A. Troisi, How Quasi-Free holes and Electrons are Generated in Organic Photovoltaic Interfaces, *Faraday Discuss.* 2013, **163**, 377-392.

[65] H. Ma and A. Troisi, Direct Optical Generation of Long-Range Charge-Transfer States in Organic Photovoltaics, *Adv. Mater.* 2014, **26**, 6163-6167.

[66] A. A. Bakulin, A. Rao, V. G. Pavelyev, P. H. M. van Loosdrecht, M. S. Pshenichnikov, D. Niedzialek, J. Cornil, D. Beljonne, and R. H. Friend, The Role of Driving Energy and Delocalized States for Charge Separation in Organic Semiconductors, *Science* 2012, **355**, 1340-1344.

[67] H. Huang, W. Chen, S. Chen, D. C. Qi, X. Y. Gao, and A. T. S. Wee, Molecular Orientation of CuPc Thin Films on C_{60}/Ag(111), *Appl. Phys. Letts.* 2009, **94**, 163304.

[68] B. P. Rand, D. Cheyns, K. Vasseur, N. C. Giebink, S. Mothy, Y. Yi, V. Coropceanu, D. Beljonne, J. Cornil, J.-L. Bredas, and J. Genoe, The Impact of Molecular Orientation on the Photovoltaic Properties of A Phthalocyanine/Fullerene Heterojunction, *Adv. Funct. Mater.* 2012, **22**, 2987-2995.

[69] A. L. Ayzner, D. Nordlund, D. H. Kim, Z. N. Bao, and M. F. Toney, Ultrafast Electron Transfer at Organic Semiconductor Interfaces: Importance of Molecular Orientation, *J. Phys. Chem. Letts.* 2015, **6**, 6-12.